DISCOVERY

Morphological effect of surface modified, nanoflower and nanotube zinc oxide catalysts for biodiesel production

Kamaluddeen Suleiman Kabo[1], **Abdul Rahim Yacob**[2], **Muhammad Suleiman Darma**[1*], **Bello Oluwasesan Michael**[1], **Ikechukwu Ogadimma Alisi**[1], **Abdu Muhammad Bello**[3]

To Cite:
Kabo KS, Yacob AR, Darma MS, Michael BO, Alisi IO, Bello AM. Morphological effect of surface modified, nanoflower and nanotube zinc oxide catalysts for biodiesel production. *Discovery* 2023; 59: e37d1036

Author Affiliation:
[1]Department of Applied Chemistry, Federal University Dutsin-Ma, Katsina, Nigeria
[2]Department of Chemistry, University Technology, Malaysia
[3]Department of Chemistry, Kano University of Science and Technology, Wudil, Nigeria

[*]**Corresponding Author**
Department of Applied Chemistry, Federal University Dutsin-Ma, P.M.B 5001, Katsina State
Nigeria
Email: smdarma@fudutsinma.edu.ng

Peer-Review History
Received: 20 February 2023
Reviewed & Revised: 24/February/2023 to 06/March/2023
Accepted: 09 March 2023
Published: April 2023

Peer-Review Model
External peer-review was done through double-blind method.

Discovery
pISSN 2278–5469; eISSN 2278–5450

ABSTRACT

Biodiesel is an alternative biofuel that could help to reduce the use of fossil fuels and protect the environment. However, its production is still challenged by catalyst development, evaluation and process optimization. In this research, surface modified nanoparticles (SM-ZnO), nanoflowers (NF-ZnO) and nanotubes (NT-ZnO) Zinc oxide catalysts were developed and used in the methanolysis production of biodiesel from rice bran oil (RBO) without any doping at catalyst loading of 3.7%, methanol to oil ratio 1:9, temperature of 65^{o}C and reaction time 180 mins. Catalysts were characterized by field emission scanning microscopy (FESEM), X-ray powder diffraction (XRD), Fourier transform Infra-red (FTIR) and basic concentration back titration analyses and biodiesel yield was calculated using NMR analysis. Results obtained show that the nanoparticles were successfully prepared from direct precipitation, nanoflowers and nanotubes through hydrothermal method without the use of any surfactant or templating agent. Moreover, the results of transesterification activity of the nano structured compounds showed that commercially available ZnO has biodiesel yield of 8.37%, nanoparticles 35.34%, nanoflowers 34.27% and nanotubes 42.35%. Thus, the above structure modifications helped in the preparation of new transesterification catalysts with increased activity in comparison to commercial one, the best being nanotubes which demonstrated highest biodiesel conversion and suitability for use at lower reaction conditions.

Keywords: Nanoparticles, Nanoflowers, Nanotubes, Methanolysis, Rice bran oil, Biodiesel, Structure modification.

1. INTRODUCTION

Biodiesel is a clean and renewable fuel which is considered the best substitution for diesel fuel. The advantage of this biofuel over the conventional diesel fuel includes: High cetane numbers, low smoke and particulates, low carbon dioxide

DISCOVERY SCIENTIFIC SOCIETY

and hydrocarbon emissions; it is biodegradable and nontoxic. It has low carbon monoxide (CO), unburned hydrocarbons (HC) and smoke emissions. The limited and fast diminishing resources of fossil fuel, increasing price of crude oil and environmental concern have been diverse reasons for exploring the use of vegetable oil as an alternative fuel (Jauro and Adams, 2011).

However, biodiesel when produced in good quality can be used both in mixed and pure form on current diesel engines. Production of biodiesel is easy, but the major challenges with biodiesel remain with the availability of cheap raw materials and optimization of the catalyst for better activity to make the process commercially viable. Many works on homogeneous and heterogeneous biodiesel production processes were reported. However, heterogeneous catalysts are prepared due to problems associated with homogeneous catalysts which their use as catalysts causes environmental damage and high cost of biodiesel. Heterogeneous basic catalysts were found to be better compared to heterogeneous acid catalysts in biodiesel production. Metal oxides are mostly used because of their ability to supply positive metal ions which will attract ethanol to form metallic alkoxides that would attack the triglyceride oil molecules, leading to its final conversion to ester or biodiesel. However, most of them have low activity or deactivate easily, which necessitate the use of various modification processes to improve their performance. Modifications could be achieved through doping, coprecipitation, or structural modification, all with the aim of exposing catalyst active sites for better performance. Environmentally benign oxides like zinc oxide could be modified to serve as heterogeneous catalysts (Molina, 2013).

Information from many literatures have shown that many works were carried out to produce biodiesel as an alternative energy source and study the effects and optimization of the reaction parameters; properties and amount of catalyst, nature and quantity of oil, time and temperature on its yield, physical and chemical properties. However, from the available literature, no focus is given to the optimization of catalysts' the structural modification process prior to application. This will help to reduce both material personal cost and ease catalyst assessment for commercial applications. It is expected that the catalytic activity of zinc oxide will be influenced by structural modification due to structural differences associated with nanoparticles, nanoflowers and nanotubes. The structural modification of zinc oxide will have significant effect on the catalyst activity; biodiesel yield and catalyst stability; reusability and leaching.

The prospect of using nanostructured materials for improved performance in biodiesel production is reported in the literature. The use of K-doped sodium titanate nanotubes was reported by (Hernández-Hipólito et al., 2015). 3.3% K-doped sodium titanate was able to yield 94-96% conversion at 80°C in just 1 h. Shuit et al., (2013) highlighted the possibility of using carbon nanotubes (CNTs) as potential stable catalysts in biodiesel production. Shuit & Tan, (2014) used sulphonated CNTs in the esterification reaction carried out at 170°C for 3 h at a methanol to palm fatty acid distillate ratio of 20 and catalyst loading of 2 wt% in a pressurised reactor with a corresponding yield up to 93.4%. The catalysts were stable and could be reused (Alhassan et al., 2014). Synthesis of Ferric–Manganese Doped Tungstated Zirconia nanoparticles as heterogeneous superacid catalyst for biodiesel Production from waste cooking oil. Highest biodiesel yield of 96% was achieved at the optimized conditions of reaction temperature of 200°C; stirring speed of 600 rpm, 1:25 molar ratio of oil to alcohol and 4% w/w catalyst loading. From the above literature, it can be observed that emphasis was given to the use of dorpants and higher reaction conditions to increase the catalyst' activity. In this research, zinc oxide nanostructures were prepared and used in transesterification without any doping under mild reaction conditions to evaluate the effect of structural modification in their catalytic activity towards transesterification reaction of rice bran oil to produce biodiesel.

2. MATERIALS AND METHODOLOGY

All Chemicals and reagents used in this research were analytical grade and used with no further purification.

Zinc oxide Surface Modification

Surface modified ZnO was prepared via hydration dehydration of commercial ZnO followed by calcination. Hydration was done by weighing 12.0g of the commercial zinc oxide sample, mixed with 150 ml distilled water in a 250 ml round bottom flask and refluxing at 95°C for 12 h. The hydrated ZnO obtained after reflux was vacuum-filtered, dried in an oven at 105°C overnight to remove the excess water. The surface modified ZnO labelled as SM-ZnO was then calcined in a furnace at 400°C for 2 hrs (Niju et al., 2014). This reaction scheme is simply depicted in Equation 1 and 2.

$$ZnO_{(s)} + H_2O_{(l)} \xrightarrow{reflux} Zn(OH)_{2(s)} \qquad \text{eq (1)}$$

$$Zn(OH)_{2(s)} \xrightarrow{Calcination} ZnO_{(s)} + H_2O_{(g)} \qquad \text{eq (2)}$$

Preparation of Zinc Oxide Nanoflowers

Zinc oxide nanoflowers were synthesized via solvothermal method (Chakraborty et al., 2015). 0.25 M Zinc acetate solution and sodium hydroxide solution were prepared in deionized water at room temperature. Zinc acetate solution was gently heated to 80°C, the NaOH solution was slowly added under vigorous stirring until the pH reached 11 with the formation of white precipitate. The precipitate was poured into a Teflon lined sealed stainless steel autoclave and heated at 120°C for 4 hrs, after which the autoclave were allowed to cool down to room temperature. The precipitate was centrifuged, washed several times with distilled water and then dried at 60°C for 12 hrs. The Zinc oxide nanoflower obtained was labelled as NF-ZnO.

Preparation of Zinc Oxide Nanotubes

ZnO nanotube was prepared using solvothermal method as reported by (Sin et al., 2015). Ethanolic solutions of 0.25 M Zinc acetate and 0.5 M NaOH were appropriately prepared. The NaOH solution was slowly introduced into the zinc acetate solution under magnetic stirring at 60°C for 30 min. Excess NaOH solution was used until a pH of 11 was reached and a suspension was obtained. The suspensions were allowed to cool and transferred to Teflon linen stainless steel autoclave, placed in a furnace at 140°C for 8 hrs. The precipitate was collected, washed with methanol and dried at 60°C in air for 12 hrs. This sample was labelled NT-ZnO.

Catalysts Characterization

Field Emission Scanning Electron Microscopy (FESEM) method was used to study the morphology and estimate the particulates size of Both the SM-ZnO, NF-ZnO and NT-ZnO catalyst samples. The X-ray powder diffraction (XRD) was used to identify the crystalline phases of the catalyst samples by means of lattice structural parameters and to estimate the crystallite size and crystallinity. Fourier Transform Infra-Red spectroscopy (FT-IR) was employed to study the various functional groups. Nitrogen adsorption on surfaces is used to determine the surface area, pore size and pore distribution of catalyst materials Basic Strength Back Titration Analysis.

The basic strength and the amount of basic site of the prepared catalyst samples were studied using basic titration analysis. In this method, the basicity of the base is reported as the acidity of the conjugate acid and vice versa. The basic catalysts were neutralized with a known concentration of HCl by an equivalent amount of its basicity. As a result, the original concentration of HCl was reduced. The excess HCl is treated with known concentration of NaOH and the amount of NaOH reacted is equivalent to the amount of basicity of the catalyst (Kaur & Ali, 2014). The measurement of the basicity was conducted by mixing 0.2 mg of the catalyst samples shaken in 10 mL of distilled water and left for 24 hrs. The filtrate obtained was separated by a centrifuge and the resulting solution was neutralized with 10 ml of 0.05 M HCl. Subsequently, the remaining acid was titrated with 0.02 M NaOH and phenolphthalein was employed as an indicator. The various amounts were determined using the stoichiometric relationship.

Biodiesel Preparation and Analysis

Biodiesel was prepared via transesterification reaction of Rice Bran Oil (ROB) with methanol (methanolysis) at optimum reaction conditions of catalyst loading of 3.7% methanol to oil ratio 1:9, temperature of 65°C and time of 180 min. The prepared catalysts were used in the reaction and their activity was evaluated in terms of percentage conversion which was determined by NMR (Morgenstern et al., 2006).

Transesterification of RBO to Produce Biodiesel

In this experimental set-up, a 250 ml double-necked round bottomed flask is fitted with a condenser connected to flowing water and a thermometer, then mounted onto retort stands and slowly immersed in a bath of paraffin oil placed on a hot plate. An appropriate amount of methanol is measured into the round flask followed by the needed amount of catalyst. This is then vigorously stirred for 20 min with the aid of a magnetic stirrer to form a uniform alkoxide mixture. 20 ml of rice bran oil was then added and the set-up was heated in paraffin oil at 65°C under magnetic stirring for a specific period of time. The product was then allowed to settle overnight and centrifuged, after which three distinct layers were observed. The small upper layer of unreacted methanol was removed, the middle layer of biodiesel was carefully decanted from the lower layer which contains glycerol and the residual solid catalyst.

3. RESULTS AND DISCUSSION

Catalysts Preparation

The surface properties of commercially available zinc oxide were improved by hydration-dehydration technique, the nanoflowers and nanotubes were grown by hydrothermal growth. During the precipitation process, the formation of soluble Zn^{2+} species in form hydroxide complexes such as $Zn(OH)_{2(aq)}$ and $[Zn(OH)_4]^{2-}{}_{(aq)}$ usually occurs at pH > 9, according to the reaction Equation 3.

$$Zn^{2+}_{(aq)} + 2HO^{-}_{(aq)} \longrightarrow Zn(OH)_{2(aq)} \longrightarrow ZnO_{(s)} + H_2O_{(l)} \quad \text{eq (3)}$$

With increasing pH and higher OH^- concentration, the equilibrium shifts to the right as in Eqaution 4, thereby favoring the formation of solid ZnO usually within the range of 13 ≤ pH ≥ 9 (Yamabi & Imai, 2002).

$$HO^- + HO^- \rightleftharpoons O^{2-} + H_2O \quad \text{eq (4)}$$

The formation of ZnO nanoparticles happened at higher pH of around 11. The availability of ^-OH ions leads to the formation of $[Zn(OH)_4]^{2-}$ which serve as the growth unit of ZnO structures. The higher pH value results in the formation of more $[Zn(OH)_4]^{2-}$ which covers the preferential growth axis in ZnO plane and prevents its nucleation. As a result, ZnO loses its preferred plane of growth leading to disordered growth and the formation of small nanoparticles. There was no crystal growth during the precipitation, Zn^{2+} ions where immediately precipitated and so no nucleation occurred leading to the production of nanoparticles. The optimum concentration of Zn^{2+} in the solution under hydrothermal growth condition leads to the nucleation along the prepared site, which results in its growth to have a particluar shape (Guo et al., 2005).

For nanoflowers, the flower-shaped structures are constituted by the accumulation of several hundreds of sharp-tipped hexagonal zinc oxides. The growth of nanoflower started to nanoflowers that rose from a single centre arranged in a spherical shape revealing flower-like morphology. The rod tip appears sharp with wide hexagonal bases. The growth process of the flower-shaped ZnO nanostructures composed of hexagonal nanoflowers was caused the initial precipitation of $Zn(OH)_2$. This $Zn(OH)_2$ obtained dissolves significantly in water to yield the Zn^{2+} and OH^- ions (Wu et al., 2008). Therefore, as the concentration of these ions goes beyond the critical value, the precipitation of ZnO nuclei is initiated. Thus, the ZnO nuclei concentration increases arranging themselves in a flower-shaped structure, due to surface energy. The hexagonal nanoflowers with six defined facets arose to maintain the minimum surface energy so as to keep the symmetry of the crystal structure (wurtzite ZnO).

The growth of the new crystals increases the phase boundaries at a certain speed and eventually gets contact with each other, starting the base of structure. As soon as the base is formed, the growth rates starts to decrease along the transverse direction and growth in the radial direction continues being the top surface energetically favored surface. The formation of tip at the edge is attributed to the different growth velocities in dissimilar growth planes. The growths are also reliant on the growth velocities of different growth planes in the ZnO crystal in a manner that the higher the growth rate, the quicker the disappearance of the plane, which leads to the pointed shape in end of the c-axis (Wahab et al., 2007).

Nanotubes are formed from nanorods by etching as a result of selective dissolution of the metastable ZnO rich (0 0 1) polar face in the presence of strong base (Gan et al., 2009). Under relatively high pH compared to nanoflowers, ZnO is constantly attacked by hydroxide ions, resulting in etching of the nanorods and subsequent transformation to nanotubes (Breedon et al., 2009). Under our experimental conditions, without the use of any surfactant or structure directing agent, nanotubes were grown as shown in Figure 3.

Characterization

Field Emission Scanning Electron Microscopy (FESEM)

The morphology and approximate particle size of the samples was examined using FESEM analysis. The result shows the formation of various types of ZnO which largely depends on the conditions used during the precipitation (Kawano & Imai, 2008). The FESEM micrographs of the different ZnO samples are shown in Figures 1, 2 and 3. From Figure 1, it can be observed that the SM-ZnO samples prepared by the hydration-dehydration method contain aggregate zinc oxide crystals of different sizes. It is similar to bulk zinc oxide because of large and irregular particle sizes similar to bulk ZnO.

In some, a long hexagonal crystal shape that is related to zinc oxide crystals could be observed with a size ranging between 100 to about 250 nm. The micrograph in Figure 2 shows the formation of ZnO nanoflowers obtained under the preparatory experimental conditions. This nanostructure is similar to those obtained by (Wahab et al., 2007; Wu et al., 2008), having average diameter of 100-300 and a length of 1000-1500nm. Figure 3 shows the formation of ZnO hollow nanotubes from NT-ZnO samples. The image shows a hollow tube of zinc oxide with an estimated thickness of 10 nm and 200 nm wide. Nanotubes obtained from this method are fully etched compared with the one reported by (Gan et al., 2009).

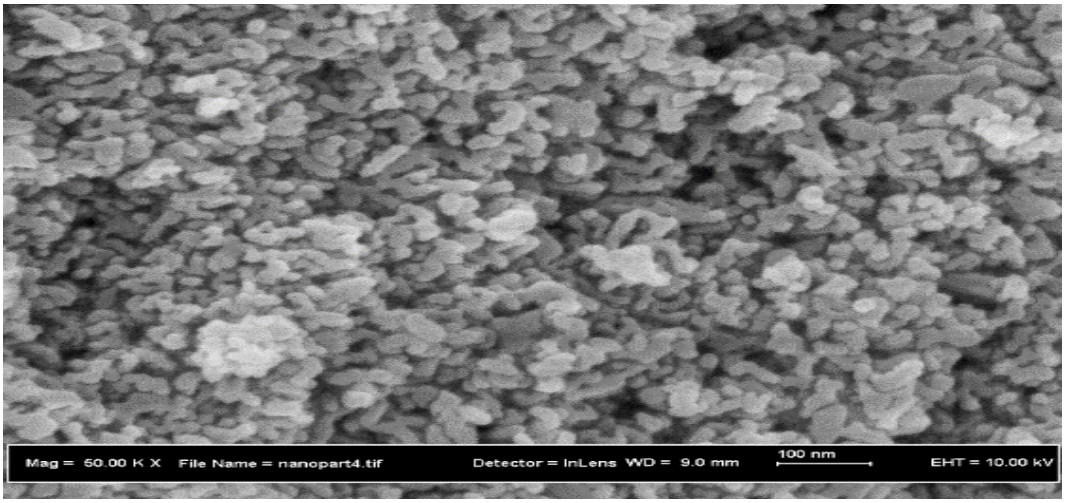

Figure 1 FESEM showing the micrographs image of SM-ZnO

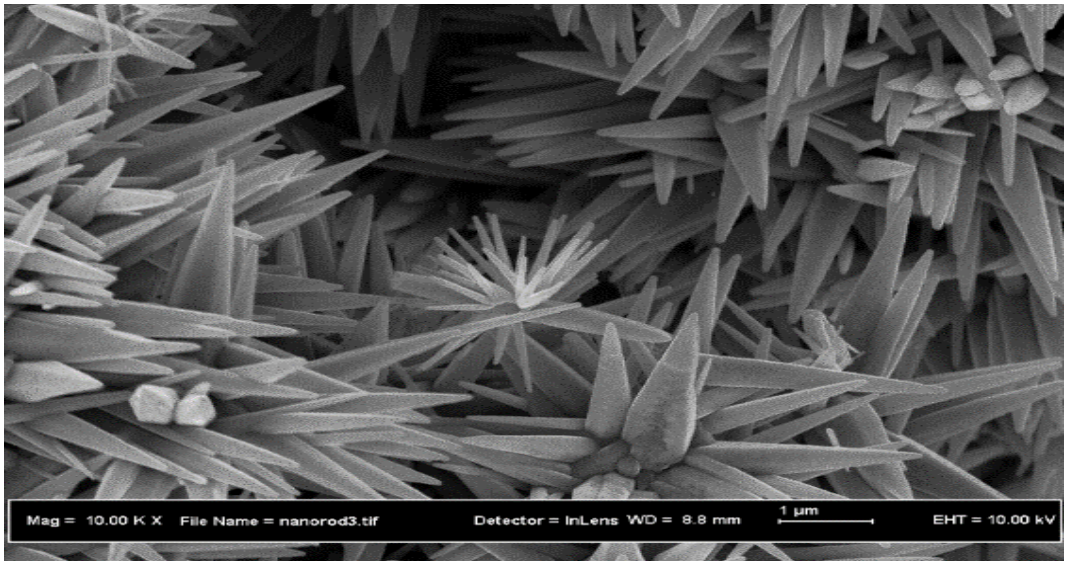

Figure 2 FESEM showing the micrographs image of NF-ZnO

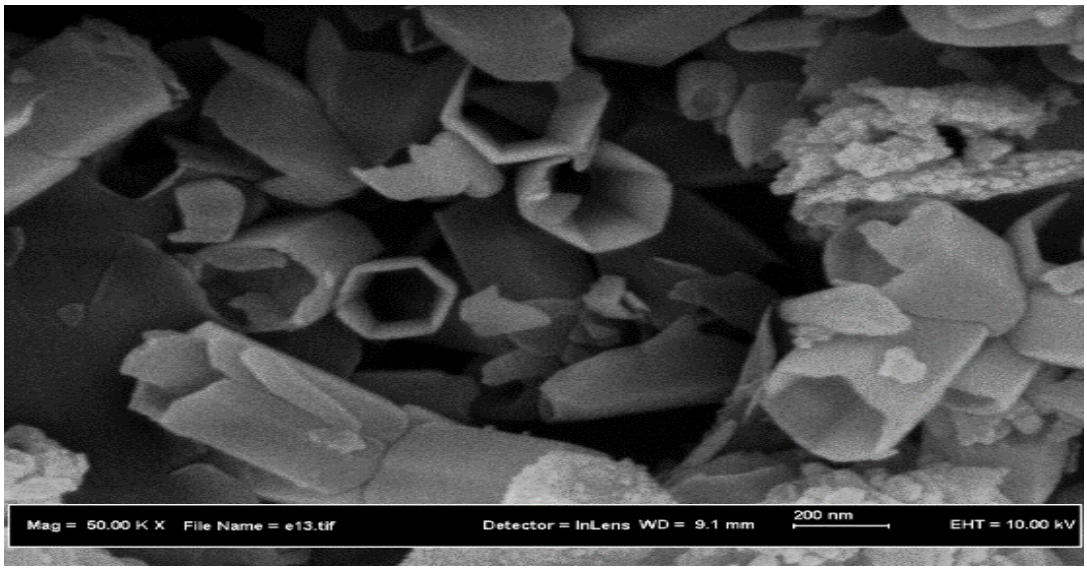

Figure 3 FESEM showing the micrographs image of NT-ZnO

X-Ray Powder Diffraction (XRD)

The X-ray diffraction patterns of the synthesized SM-ZnO, NP-ZnO, NF-ZnO and NT-ZnO in figure 4 show the formation of hexagonal wurtzite ZnO type with lattice parameters a = 0.3296 and c = 0.52065 nm irrespective of their preparatory methods. However, the shapes and size of the individual samples obtained differ indicating their morphological differences as already observed from the FESEM micrographs. The XRD pattern of SM-ZnO consists of the prominent peaks associated with hexagonal wurtzite zinc oxide structures along hkl planes of (100), (002), (101), (102), (110), (103), (200), (112) and (201). However, variations were observed regarding their 2θ positions, peak width and intensities, which could be attributed to their size and morphological differences. Scherer's formula (Equation 5) was used in calculating the average crystallite size of the first three most intense peaks.

$$L = \frac{k\lambda}{\beta \cos\theta} \qquad \text{eq (5)}$$

Where; L is a measure of the dimension of the crystal in the direction perpendicular to the reflecting plane, λ is the X-ray wavelength, β is the peak Full Width at Half Maximum (FWHM), θ is the angle between the beam and the normal to the reflecting plane and K is a constant (often taken as 1).

The diffraction pattern of SM-ZnO in Figure 4 (a) is indexed as ZnO zincite, with JCPDS reference number 01-075-1526 having peaks appearing at 2θ positions 31.8216, 34.4811, 36.3117, 47.5940, 56.6326, 62.8751, 66.4041, 67.9761 and 69.1051. The 3 prominent peaks at 2θ positions 31.8216, 34.4811, and 36.3117 are high with corresponding low width, indicating that a is the most crystalline with relatively large crystallite size. The average crystallite size was calculated as 48.99 nm, which is lower than observed in the FESEM because the particle size observed from the FESEM may consist of an aggregate of other small crystals. The diffraction pattern of NF-ZnO in Figure 4 (c) is matched with that of zincite synthetic JCPDS pdf card number 01-089-1397 with peaks at 2θ positions of 31.8457, 34.5131, 36.3263, 47.5658, 56.6162, 62.9324, 66.5319, 68.0260 and 69.1296. The 3 prominent peaks appeared at 2θ positions of 31.8457, 34.5131, and 36.3263. A slight shift in the 2θ position together with a decrease in the peak width to nearly similar to SM-ZnO indicates a structural differences and increase in the particle size compared to nanoparticles.

The intense peak also indicate that nanoflowers are highly crystalline (Wu et al., 2007). Average crystallite size was calculated as 41.17 nm which is lower than observed in FESEM. This is because the nanoflower consist of aggregates of smaller crystals. The diffraction pattern of NT-ZnO in Figure 4 (d) matched with that of zincite synthetic, JCPDS pdf card number 01-071-6424 with peaks at 2θ positions of 31.7849, 34.4274, 36.2537, 47.6214, 56.6065, 62.7673, 66.4634, 67.9772 and 69.0993. The 3 prominent peaks appeared at 2θ positions of 31.7849, 34.4274 and 36.2537. Similaritys of the index card number with that of nanoflowers indicates that nanotubes are developed directly from the same source; nanorods as a result of etching process (Breedon et al., 2009; Gan et al., 2009). However, a slight shift in the 2θ position together with the increase in peak width indicates structural difference and decrease in the particle size compared with nanoflowers which is aggregate of nanorods. The peaks are less intense also indicating that the nanotubes are less crystalline. Average crystallite size was calculated as 29.96 nm, which also shows that its aggregate particles are smaller than SM-ZnO and NF-ZnO.

Fourier Transform Infra-Red Spectroscopy (FTIR)

FTIR spectra of SM-ZnO and ZnO nanostructure samples were recorded before and after the modification. The results are in agreement with FESEM and XRD analyses as the spectra obtained are consistent with those of ZnO samples reported in the literature. From the spectra of SM-ZnO in Figure 5 (a), the result shows the presence of two types of OH bonding in the spectra; OH stretching and OH bending. The OH stretching appeared at 3420 cm-1 and the bending at 1520 cm-1; these peaks are due to the adsorbed water on the interlayer spaces. The band at 1050cm-1 is due to OH bending. The bands at 740, 695, 525 cm-1 are due to Zn-O lattice vibration bands (Li et al., 2012; Oswald, 1971). 2035 cm-1 is due to atmospheric CO2 while 850 cm-1 could be due to the presence of nitrates or sulphates impurities (Seredych et al., 2012).

For NP-ZnO in Figure 5 (b), FTIR peaks attributed to ZnO nanoparticles as obtained by (Hong et al., 2006) were observed. The peaks appear within the range of 3500-2900 cm^{-1} and 1570 cm^{-1} are related to ^{-}OH. The appearance of these peaks even at 800^{o}C indicted that the hydrogen was chemically bonded to oxygen within ZnO network. The intense peak at 490 and the other at 710 are both attributed to ZnO stretching modes (Prakoso, 2012). The peak at 880 is due to C-H and the others at 1790 due to C=O stretch are attributed to the adsorbed esters used in the preparation. The strong peak of ZnO appeared 550 cm^{-1}.

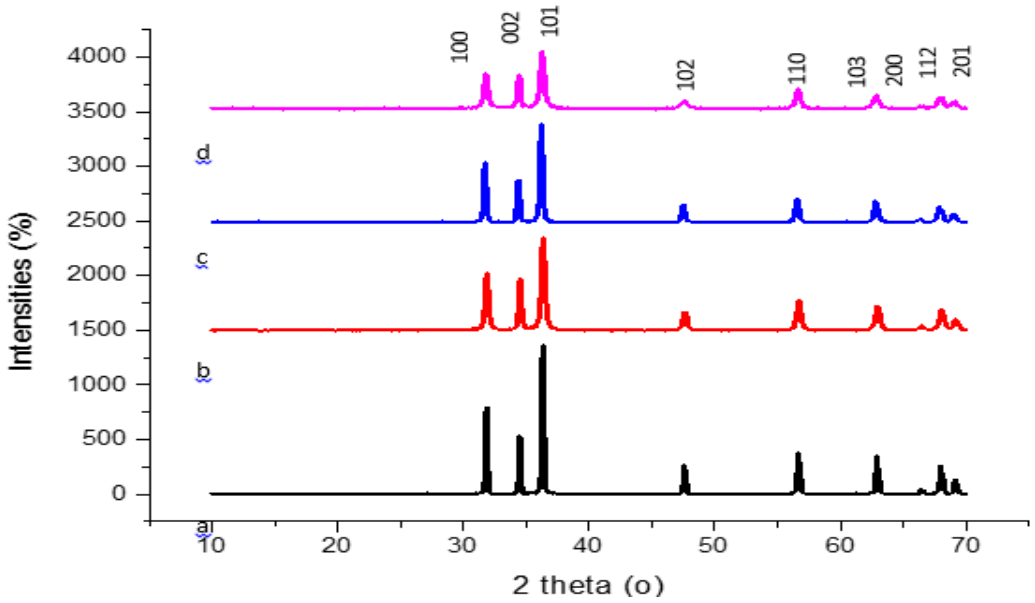

Figure 4 XRD diffraction patterns of ZnO samples prepared; (a) SM-ZnO, (b) NP-ZnO, (c) NF-ZnO, and (d) NT-ZnO

The FTIR spectrum of NF-ZnO in Figure 5 (c) also show the peak of ZnO nanoflowers as reported by (Wu et al., 2006) having characteristic -OH at 3500-2900 and 1640-1540 cm^{-1} related to OH^-. 720, 580 and 550 are related to ZnO (Wahab et al., 2007), 2300 cm^{-1} is due to adsorbed CO_2, NT-ZnO spectrum in Figure 5 (d) are nearly similar with that of nanoflowers having absorption bands at 3500-2900 cm^{-1} and 1630-1450 cm^{-1} associated with -OH. 2300 cm^{-1} due to adsorbed CO_2, 860 and 694 cm^{-1} related to ZnO. The similarity of this spectrum with the one recorded from nanoflowers is due to the fact that nanotubes are directly developed from nanoflowers as a result of the etching process. However, the peaks associated with ZnO are more intense in nanotubes suggesting an increased exposure of polar Zn^{2+}- O^{2-} bond in nanotubes as compared to nanoflowers.

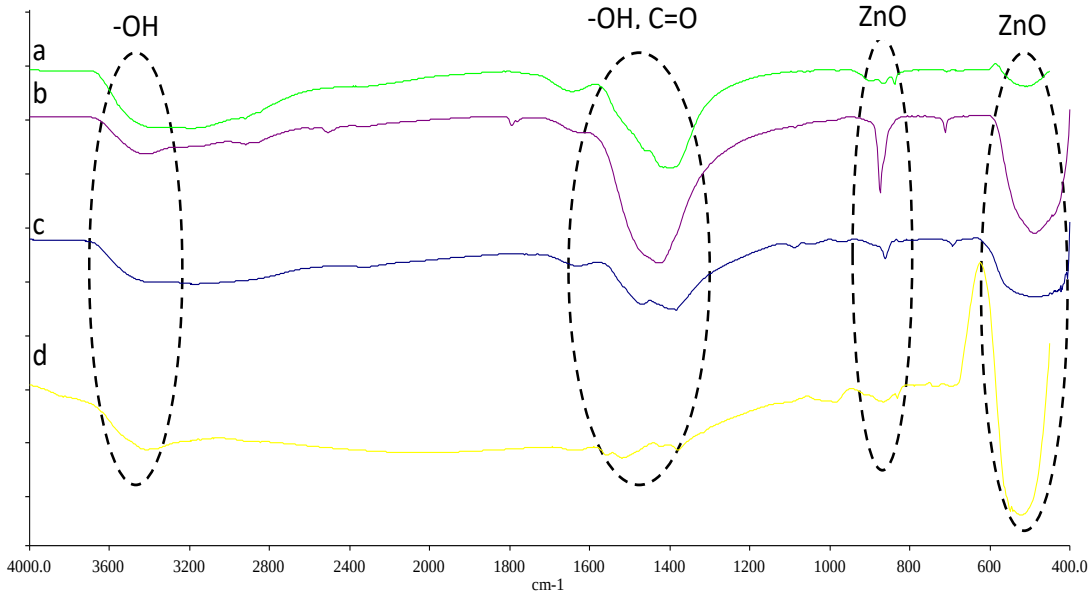

Figure 5 FTIR spectra for ZnO (a) SM-ZnO (b) NP-ZnO (c) NF-ZnO (d) NT-ZnO

The FTIR results are in agreement with FESEM and XRD as the spectra recorded are consistent with those of ZnO nanostructures reported. The main peaks associated with the hydroxyl groups could still be observed in the spectra but (Prakoso, 2012) also reported their presence even when the samples were calcined to 800°C and inferred that they are chemically bonded on the oxygen in the ZnO lattice. Also the broad peak at 550cm^{-1} associated with ZnO is present in all samples. The intensity of this peak also agrees with FESM and XRD because it shows the more sharp and intense it is, the higher the crystallinity and particle size

and vice versa. Moreover, peaks associated with COO^- asymmetric stretching due to carboxylate from the acetic groups and CO stretch, due to adsorbed CO_2 were also observed.

Basic Sites Concentration Back Titration Analysis

The basic strength of the prepared samples was determined through basic back titration. The basic site of the prepared commercial ZnO before hydration was determined as 1.365 mmol/g (Yacob & Kabo, 2015). However, after the process, an increase was observed as the basic site was determined as 1.753 mmol/g due to the creation of vacant pores and defects as a result of interaction and removal of water that occurred. This method was used to improve the basicity of CaO which was used in transesterification resulting in 94.25 % oil to biodiesel conversion (Niju et al., 2014). The basic site of the synthesized nanostructures were determined as 2.41 for NP-ZnO, 2.19 NF-ZnO and 2.73 mmol/g for NT-ZnO respectively.

It can be observed that the basic sites of zinc oxide nanostructures are significantly higher than that of surface modified commercial ZnO. The development of ZnO nanostructures is associated with the direction and rate of crystal growth along its favorable growing planes. Usually, the growth of ZnO is favored at the stable, nonpolar 0001 plane along the c-axis leading to the hexagonal ZnO structure consisting of zinc and oxygen ions coordinated tetrahedral. However, the development of nanostructures can lead to growth along other directions that are polar (Baruah & Dutta, 2009). This can lead to the development of various morphologies and exposure of polar zinc oxide surfaces resulting in the observed increase in basic sites due to structural differences (Nambo et al., 2015).

Based on this, the development of ZnO nanotubes favors the growth in other polar directions with highest exposure of Zn^{2+} and corresponding value of basic sites increase compared to the other nanostructures. Followed by nanoparticles and finally nanoflowers. This is supported by XRD analysis, beacues 001 peak is associated with c-axis. It could be observed from XRD spectra (Figure 5) that nanotubes ZnO have the lowest intensity of 001 peak indicating decreased growth along the non-polar c-axis. The trend of intensity associated with non-polar c-axis follows; nanotubes lowest, then nanoparticles, then nanoflowers then surface modified commercial. This can further be supported by nitrogen adsorption analysis. Nanotubes have the highest BET surface area, followed by nanparticles and then nanoflowers and finally modified commercial. This shows that nanotubes with highest textural properties have the corresponding highest basic sites. Followed by nanparticles, nanflowers and surface modified commercial. Thus, the trend of increase in basic site concentration could be due to both structural development as observed from XRD and superior textural properties as observed from nitrogen adsorption (NA) analysis.

Biodiesel from Structure Modified Catalysts

Surface modified ZnO prepared nanostructures were used in the methanolysis reaction in to determine their transesterification yield. The conditions for the reaction were: Methanol to oil ratio 12:1, catalyst loading 5%, temperature 65°C and time 4 h. The result indicates that the surface modified zinc oxide which is from commercial source oil to biodiesel conversion of only 8.37%. However, the structural modification of ZnO shows increase in the catalytic activity towards transesterification. NP-ZnO produced biodiesel conversion of 35.34%, NF-ZnO 34.27% and NT-ZnO 42.35%. The summary of the results is presented in table 1.

Table 1 Summary of biodiesel conversion obtained from modified ZnO catalysts

Catalyst Type	Catalyst Name	Time of reaction (mins)	Biodiesel Yield (%)
Surface-Modified Commercial	SM-ZnO	180	8.37
Nanoparticles	NP-ZnO	180	35.34
Nanoflowers	NF-ZnO	180	34.27
Nanotubes	NT-ZnO	180	42.35

The trend (Table 1) shows that SM-ZnO has the lowest conversion. However, there was an increase for all ZnO nanostructures used. Among them, nanotubes have the highest followed by nanoparticles and finally nanoflowers. This result is in complete agreement with the characterization results. It was observed that the development of nanotubes favors its crystal growth along the polar axis, thereby exposing the polarity Zn^{2+}-O^{2-} bond more which resulted in its increased activity during the reaction. The same phenomenon are also responsible for the increased observed in nanoparticles and nanoflowers. The higher conversion observed in nanoparticles and nantubes was due to its smaller crystal size compared to nanoflowers which provided greater surface area available for contact with reactants. This can also be supported from the nitrogen adsorption analysis, nanotube ZnO have superior

textural properties; BET surface area, pore size and pore volume, all of which could have a significant effect on the increase in catalyst activity.

Table 2 Comparison of catalyst properties and their corresponding biodiesel conversion

Catalyst Type	Catalyst Name	Particle Size (nm)	Basic Sites ($mmolg^{-1}$)	Biodiesel Conversion (%)
Surface-modified ZnO	SM-ZnO	48.99	1.45	8.37
Nanoparticles ZnO	NP-ZnO	34.32	2.41	35.34
Nanoflowers ZnO	NF-ZnO	41.17	2.19	34.27
Nanotubes ZnO	NT-ZnO	29.96	2.73	42.35

However, the conversions obtained from both surface modified and synthesized nanostructure ZnO are low. The implication of the results obtained show a marked increase in activity on oil to biodiesel conversion from just 8.38% from commercial to 42.35% from nanotubes.

4. CONCLUSION

Among the catalysts' properties evaluated, it can be deduced that the amount of basic sites is directly proportional to the biodiesel conversion. The results indicated that the single most important parameter responsible for biodiesel conversion is the catalysts' basic sites. Moreover, their structural properties are a contributing factor in their activity as well. The superior textural properties associated with ZnO nanotubes help to make it the most active among the catalysts. Thus, the use of different ZnO structures in transesterification shows that the structural modification alone can have a positive effect on basic sites and corresponding biodiesel conversion. Although the conversion using nanostructured ZnO samples was still lower than required but considering the mild reaction conditions used, the result is remarkable, underscoring the significance of structural modifications for increasing the activities of catalysts without the addition of excess basic or acidic modifiers that can lead to leaching and eventual toxicity.

Informed consent: Not applicable.

Ethical approval
Not applicable.

Conflicts of interests
The authors declare that there are no conflicts of interests.

Funding
The study has not received any external funding.

Data and materials availability
The Zinc oxide, Rice bran oil and other chemicals data used to support the findings of this study are available from the corresponding author upon request.

REFERENCES AND NOTES

1. Alhassan FH, Rashid U, Yunus R, Sirat K, Ibrahim LM, Science C, Putra U. Synthesis of Ferric – Manganese Doped Tung stated Zirconia Nanoparticles as Heterogeneous Solid Superacid Catalyst for Biodiesel Production from Waste Cooking Oil. Int J Green Energy 2014; 37–41. doi: 10.1080/1543 5075.2014.880843
2. Baruah S, Dutta J. Hydrothermal growth of ZnO nanostructures. Sci Technol Adv Mate 2009; 10:1–18. doi: 10.10 88/1468-6996/10/1/013001
3. Breedon M, Rix C, Kalantar-zadeh K. Seeded growth of ZnO nanorods from NaOH solutions. Mater Lett 2009; 63(2):249–25 1. doi: 10.1016/j.matlet.2008.10.001
4. Chakraborty S, Tiwary CS, Kumbhakar P. Simple chemical aqueous synthesis of dahlia nanoflower consisting of finger-like ZnO nanorods and observation of stable ultraviolet photoluminescence emission. J Phys Chem Solids 2015; 78:84–89. doi: 10.1016/j.jpcs.2014.10.022

5. Gan X, Li X, Gao X, Yu W. Investigation on chemical etching process of ZnO nanorods toward nanotubes. J Alloys Compd 2009; 481(1–2):397–401. doi: 10.1016/j.jallcom.2009.03.013
6. Guo M, Diao P, Cai S. Hydrothermal growth of well-aligned ZnO nanorod arrays: Dependence of morphology and alignment ordering upon preparing conditions. J Solid State Chem 2005; 178(6):1864–1873. doi: 10.1016/j.jssc.2005.03.031
7. Hernández-Hipólito P, Juárez-Flores N, Martínez-Klimova E, Gómez-Cortés A, Bokhimi X, Escobar-Alarcón L, Klimova TE. Novel heterogeneous basic catalysts for biodiesel production: Sodium titanate nanotubes doped with potassium. Catal Today 2015; 250:187–196. doi: 10.1016/j.cattod.2014.03.025
8. Hong R, Pan T, Qian J, Li H. Synthesis and surface modification of ZnO nanoparticles. J Chem Eng 2006; 119(2–3) :71–81. doi: 10.1016/j.cej.2006.03.003
9. Jauro A, Adams MH. Production and biodegradability of biodiesel from *balanites aegyptiaca* seed oil. J Korean Chem Soc 2011; 55(4):680–684. doi: 10.5012/jkcs.2011.55.4.680
10. Kaur M, Ali A. An efficient and reusable Li/NiO heterogeneous catalyst for ethanolysis of waste cottonseed oil. Eur J Lipid Sci Technol 2014; 116:80–88. doi: 10.1002/ejlt.20130 0213
11. Kawano T, Imai H. A simple preparation technique for shape-controlled zinc oxide nanoparticles: Formation of narrow size-distributed nanorods using seeds in aqueous solutions. Colloids and Surfaces A: Physio chem Eng Aspects 2008; 319: 130–135. doi: 10.1016/j.colsurfa.2007.05.019
12. Li P, Xu ZP, Hampton MA, Vu DT, Huang L, Rudolph V, Nguyen AV. Control Preparation of Zinc Hydroxide Nitrate Nanocrystals and Examination of the Chemical and Structural Stability. J Phys Chem C 2012; 116:10325–10332.
13. Molina CMM. ZnO Nanorods as Catalyst for Biodiesel Production from Olive Oil. University of Louisville 2013.
14. Morgenstern M, Cline J, Meyer S, Cataldo S. Determination of the Kinetics of Biodiesel Production Using Proton Nuclear Magnetic Resonance Spectroscopy (1 H NMR). Energy Fuels 2006; 20(4):1350–1353. doi: 10.1021/ef0503764
15. Nambo A, Miralda CM, Jasinski JB, Carreon MA. Methanolysis of olive oil for biodiesel synthesis over ZnO nanorods. Reac Kinet Mech Cat 2015; 114(2):583–595. doi: 10.1 007/s11144-014-0802-3
16. Niju S, Meera Sheriffa Begum KM, Anantharaman N. Enhancement of biodiesel synthesis over highly active CaO derived from natural white bivalve clam shell. Arab J Chem 2014. doi: 10.1016/j.arabjc.2014.06.006
17. Oswald R. The Infrared Spectrum and Thermal Analysis of Zinc Hydroxide Nitrate. J Sep Sci 1971; 255:252–255.
18. Prakoso SP. Synthesis and Spectroscopic Characterization of Undoped Nanocrytalline ZnO Particles Prepared by Co-Precipitation. Mater sci appl 2012; 03(08):530–537. doi: 10.423 6/msa.2012.38075
19. Seredych M, Mabayoje O, Bandosz TJ. Visible-Light-Enhanced Interactions of Hydrogen Sulfide with Composites of Zinc (Oxy) hydroxide with Graphite Oxide and Graphene. Langmuir 2012; 28:1337–1346.
20. Shuit SH, Tan SH. Feasibility study of various sulphonation methods for transforming carbon nanotubes into catalysts for the esterification of palm fatty acid distillate. Energy Convers Manag 2014; 88:1283–1289. doi: 10.1016/j.enconman.2014.01.0 35
21. Shuit SH, Yee KF, Lee KT, Subhash B, Tan SH. Evolution towards the utilisation of functionalised carbon nanotubes as a new generation catalyst support in biodiesel production: An overview. RSC Adv 2013; 3(24):9070–9094. doi: 10.1039/C3RA 22945A
22. Sin J, Lam S, Lee K, Rahman A. Surfactant-free solvothermal synthesis of ZnO nanorods for effective sunlight degradation of 2, 4-dichlorophenol. Mater Lett 2015; 140:51–54. doi: 10.101 6/j.matlet.2014.10.067
23. Wahab R, Ansari SG, Kim YS, Seo HK, Kim GS, Khang G, Shin HS. Low temperature solution synthesis and characterization of ZnO nano-flowers. Mater Res Bull 2007; 42 :1640–1648. doi: 10.1016/j.materresbull.2006.11.035
24. Wu C, Qiao X, Chen J, Wang H. Controllable ZnO morphology via simple template-free solution route. Mater. Chem. Phys 2007; 102(1):7–12. doi: 10.1016/j.matchemphys.20 06.10.003
25. Wu C, Qiao X, Luo L, Li H. Synthesis of ZnO flowers and their photoluminescence properties. Mater Res Bull 2008; 43(7):188 3–1891. doi: 10.1016/j.materresbull.2007.07.025
26. Wu L, Wu Y, Pan X, Kong F. Synthesis of ZnO nanorod and the annealing effect on its photoluminescence property. Opt Mater 2006; 28(4):418–422. doi: 10.1016/j.optmat.2005.03.007
27. Yacob AR, Kabo KS. Effect of Calcination on the Basic Strength of Surface Modified Nano- Zinc Oxide Characterised by FTIR and Back Titration Methods. Adv Mater Res 2015; 11 07:326–332. doi: 10.4028/www.scientific.net/AMR.1107.326
28. Yamabi S, Imai H. Growth conditions for wurtzite zinc oxide films in aqueous solutions. J Mater Chem 2002; 12:3773–3778. doi: 10.1039/b205384e